

Student's T Robust Bundle Adjustment Algorithm

Aleksandr Y. Aravkin
University of British Columbia
Vancouver, BC
saravkin@eos.ubc.ca

Michael Styer
Stanford University
Stanford, CA
mstyer@cs.stanford.edu

Zachary Moratto
NASA Ames Moffett Field zachary.m.moratto@nasa.gov

Ara Nefian
Carnegie Mellon University and NASA Ames Moffett Field, CA ara.nefian@nasa.gov

Michael Broxton
Carnegie Mellon University and NASA Ames Moffett Field, CA michael.broxton@nasa.gov

Abstract

Bundle adjustment (BA) is the problem of refining a visual reconstruction to produce better structure and viewing parameter estimates. This problem is often formulated as a nonlinear least squares problem, where data arises from interest point matching. Mismatched interest points cause serious problems in this approach, as a single mismatch will affect the entire reconstruction. In this paper, we propose a novel robust Student's t BA algorithm (RST-BA). We model reprojection errors using the heavy tailed Student's t -distribution, and use an implicit trust region method to compute the maximum a posteriori (MAP) estimate of the camera and viewing parameters in this model. The resulting algorithm exploits the sparse structure essential for reconstructing multi-image scenarios, has the same time complexity as standard L_2 bundle adjustment (L_2 -BA), and can be implemented with minimal changes to the standard least squares framework. We show that the RST-BA is more accurate than either L_2 -BA or L_2 -BA with a σ -edit rule for outlier removal for a range of simulated error generation scenarios. The new method has also been used to reconstruct lunar topography using data from the NASA Apollo 15 orbiter, and we present visual and quantitative comparisons of RST-BA and L_2 -BA methods on this application. In particular, using the RST-BA algorithm we were able to reconstruct a DEM from unprocessed data with many outliers and no ground control points, which was not possible with the L_2 -BA method.

1. Introduction

Bundle adjustment is a large sparse geometric parameter estimation problem, in which parameters are 3D feature coordinates and camera poses. Classically, bundle adjustment is formulated in the nonlinear least squares framework (see [28] and sources cited within). The goal of bundle adjustment is to refine a visual reconstruction by identifying a sparse cloud of tie-point features in multiple images, matching tie-points common to several images, and adjusting camera and world point parameters simultaneously to improve the reconstruction. Prior information about camera parameters and ground control points are incorporated using the Bayesian modeling framework, and camera parameters and 3D world coordinates of the tie-point features are estimated using the matched tie-point features as data.

The motivating problem for our work in robust bundle adjustment is to produce a robust reconstruction in the presence of outliers generated due to the misidentification of tie-points across images. It is virtually impossible to ensure that automated algorithms for finding and matching tie-point features always generate correct correspondences. A single wrong identification can lead to a large phantom error which dominates other 'good' data in the least squares framework.

To derive our approach, we begin with a statistical model for the reprojection errors in pixel space as well as initial camera parameter errors and ground control point errors, and then find a maximum a posteriori estimate for this model using an implicit trust region optimization method. We model both reprojection errors and prior uncertainty on cameras and ground control points as distributed according

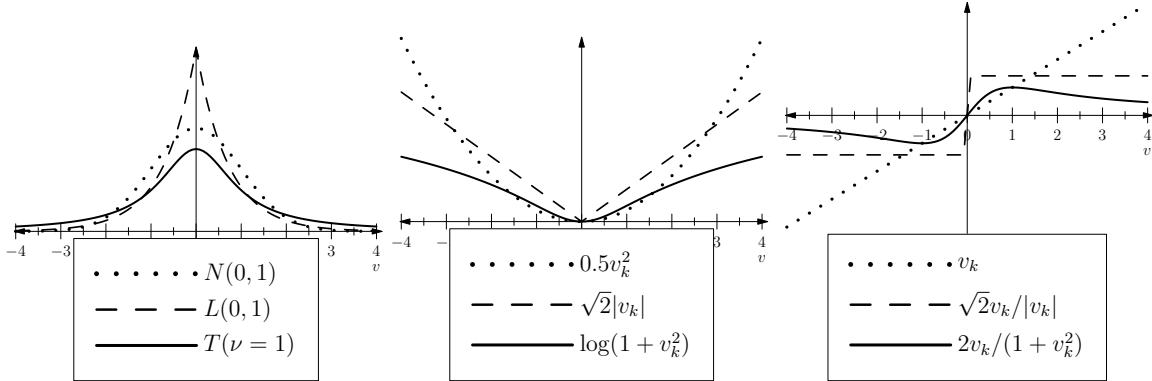


Figure 1. Gaussian, Laplace, and Student’s t Densities, Corresponding Negative Log Likelihoods, and Influence Functions (for scalar v_k)

to the Student’s t-distribution.

There are many approaches that try to incorporate the idea of ‘robust cost’ or ‘fat tails’ into the bundle adjustment framework (see [28], [11]). Most of these schemes require some iterative re-weighting of the least squares objective. However, these approaches lack a progress metric or any optimality guarantees, which limits possibilities for algorithm design and convergence criteria. We begin instead with distributional assumptions on reprojection errors, derive a corresponding *maximum a posteriori* (MAP) optimization problem, and develop an algorithm to solve it. Our approach takes advantage of the sparse structure described in [16] and [12], and determines the best camera parameters by solving a maximum likelihood (ML) problem. using an algorithm that still follows the main idea in [18] while exploiting the sparse structure in [11].

The resulting robust Student’s t BA (RST-BA) preserves the sparse structure and efficiency of the method used in [16], allowing the robust implementation to run in a comparable time to the standard BA method. Compared with automated outlier removal schemes and ad-hoc reweighting using ‘robust-cost’ functions, RST-BA is faster and more accurate both on synthetic data and in real applications. Moreover, it is straightforward to implement with minimal changes to the standard least-squares framework.

Mismatches in tie-point features is a well known problem, and there are a variety of approaches in the literature for robustification and dealing with outliers. Threshold-based outlier removal is a common approach with many variants ([27], [22], [20], [21], [4], [9], [15], [13]). After one or more iterations of bundle adjustment, observations with residuals exceeding some predetermined threshold are removed from the dataset and the bundle adjustment optimization is run again on the remaining observations. The choice of threshold depends on the particular problem and dataset. [27], for instance, uses a threshold of 1.5 standard deviations from the mean residual error, while [21] discards residuals with size to variance ratio greater than

3. Generally, some σ -edit rule is applied, with a typical range between 1 to 2 standard deviations. However, there are problems with using σ -edit rules even in the linear regression context [19, Chapter 1], and it is particularly limiting in nonlinear problems because outliers affect the initial fit, which is then used for classification of outliers and inliers.

Another common approach is iterative reweighting ([8], [7], [20], [23]). In this method, the observations are weighted at each iteration in inverse proportion to their residual errors. Observations may also be removed according to a σ -edit rule with a higher threshold [20]. Closely related to this approach is that of ‘robust cost functions’, which is discussed in [11] and implemented in [3] and [4]. The main problems with ad hoc reweighting according to such cost functions is the lack of a convergence theory that guarantees the algorithm will stop at a stationary point of the objective, and in many cases the lack of an explicit objective function.

Model-based bundle adjustment is yet another robust technique, in which prior information about the surface under reconstruction is used to aid in the adjustment [7]. [29] proposes a bundle adjustment method which does not involve solving for the camera parameters, in order to reduce numerical instability and decrease sensitivity to noise. We do not consider these approaches, since we have no prior information on the surface we are reconstructing, and refinement of the camera parameters is essential to our application.

The paper proceeds as follows. In Section 2 we formulate standard bundle adjustment as a nonlinear least squares problem that can be solved with L_2 -BA. In Section 3 we describe the multivariate Student’s t-distribution. In Section 4, we formulate robust bundle adjustment as the *maximum a posteriori* likelihood problem and develop the RST-BA algorithm to solve it. In Section 5, we use simulated data to compare RST-BA with the standard L_2 -BA algorithm, and with L_2 -BA combined with a 2-sigma edit rule for remov-

ing outliers. In Section 6, we show the results of applying the RST-BA algorithm to the problem of reconstructing lunar topography from NASA Apollo 15 orbital imagery, and compare the results with results obtained from L_2 -BA for both processed and unprocessed data.

2. Mathematical Model for BA

Suppose that we have m images taken by a moving camera, or equivalently by m cameras with different poses (locations and attitudes). Suppose that multiple tie-point features are identified in each image, and that a single feature may appear in several images. Denote by S the control network of indices describing the image tie-point matching, so that $(i, j) \in S$ if feature i was seen in image j . Let x_j denote the pose of the j th camera, and let y_i denote the 3D world coordinates of feature i . Let z_{ij} be the pixel coordinates of the projection $h(x_j, y_i)$ of feature i onto image j , ϵ_{ij} be the reprojection error $z_{ij} - h(x_j, y_i)$, and Σ_{ij} be the covariance matrix associated to ϵ_{ij} . Define x_j^0 and y_i^0 to be prior estimates of camera parameters and ground control points, with covariances Ω_j and Φ_i , respectively. All the data except for $\{x_j\}$ and $\{y_i\}$ are known and given. The standard statistical model for the BA problem is as follows:

$$\begin{aligned} z_{ij} &= h(x_j, y_i) + \epsilon_{ij} \\ \epsilon_{ij} &\sim (0, \Sigma_{ij}) \\ x_j &\sim (x_j^0, \Omega_j) \\ y_i &\sim (y_i^0, \Phi_i) \end{aligned} \quad (1)$$

The standard L_2 approach to bundle adjustment is to assume that ϵ_{ij} , x_j , and y_i are all normally distributed, and then the maximum *a posteriori* likelihood solution is equivalent to minimizing the objective

$$\begin{aligned} \min \quad & \frac{1}{2} \sum_{(i,j) \in S} [z_{ij} - h(x_j, y_i)]^T \Sigma_{ij}^{-1} [z_{ij} - h(x_j, y_i)] \\ & + \sum_j [x_j^0 - x_j]^T \Omega_j^{-1} [x_j^0 - x_j] \\ & + \sum_i [y_i^0 - y_i]^T \Phi_i^{-1} [y_i^0 - y_i] \end{aligned} \quad (2)$$

w.r.t. $\{x_j\}, \{y_i\}$.

The prior terms for camera parameters and ground control points are added to deal with gauge freedom. Ground control points can be used when 3D coordinates of certain tie-point features are well known, which is the case for Lunar topography data. Note that if there is no prior information on a particular x_j or y_i , we simply set the corresponding Ω_j^{-1} or Φ_i^{-1} to $\mathbf{0}$ in (2).

The standard approach to bundle adjustment is to minimize the objective (2) using implicit trust region methods, and in particular variants of the Levenberg-Marquardt

method are very popular (see [18], [11], [26], [25], [6] for more details on these methods). For our implementation of L_2 -BA we use a particular variant of the Levenberg-Marquardt detailed in [18, Algorithm 3.16], which is also used in the SBA implementation [16]. The method of choosing a cloud of points that ‘links’ the images together gives rise to a sparse structure, and we exploit this structure as described in [11, Algorithm A6.4].

3. Student’s t Approach

We introduce the following notation: for a vector $u \in \mathbf{R}^n$ and any positive definite matrix $M \in \mathbf{R}^{n \times n}$, let $\|u\|_M := \sqrt{u^T M u}$. We use the following generalization of the Student’s t-distribution:

$$\mathbf{p}(\epsilon|\mu) = \frac{\Gamma(\frac{s+m}{2})}{\Gamma(\frac{s}{2}) \det[\pi s R]^{1/2}} \left(1 + \frac{\|\epsilon - \mu\|_{R^{-1}}^2}{s}\right)^{-\frac{(s+m)}{2}} \quad (3)$$

where μ is the mean parameter, s is the degrees of freedom, m is the dimension of the vector ϵ , R is a positive definite matrix, and \sqrt{R} or $R^{1/2}$ denotes a Choleski factor; i.e., $\sqrt{R}\sqrt{R}^T = R^{1/2}R^{1/2} = R$. A comparison of this distribution with the Gaussian distribution assumed in (2) and the Laplace distribution appears in Figure 1. Note that the Student’s t-distribution has much thicker tails than the others, and that its influence function is re-descending (see [19] for a discussion of influence functions).

The main idea of the RST-BA algorithm is to assume that reprojection errors ϵ_{ij} come from the Student’s t-distribution (3). We also assume the Student’s t-distribution prior for the initial camera parameters $\{x_j^0\}$ and ground control points $\{y_i^0\}$. The intuition behind this approach is that extreme observations are much more likely in the Student’s t model than in the Gaussian model. Therefore, a large residual will affect the overall fit less if fitting is done in model (3). See [1] for more details.

4. Maximum Likelihood Formulation

Maximizing the likelihood for our model (1) is equivalent to minimizing the associated negative log likelihood

$$-\log \mathbf{p}(\{\epsilon_{ij}\}) - \log \mathbf{p}(\{x_j^0 - x_j\}) - \log \mathbf{p}(\{y_i^0 - y_i\})$$

Dropping the terms that do not depend on $\{x_j\}$ or $\{y_i\}$ our objective is

$$\begin{aligned} & \frac{1}{2} \sum_{(i,j) \in S} (s_{ij} + 2) \log \left[1 + \frac{1}{s_{ij}} \|z_{ij} - h(x_j, y_i)\|_{\Sigma_{ij}^{-1}}^2\right] \\ & + \frac{1}{2} \sum_j (r_j + 6) \log \left[1 + \frac{1}{r_j} \|x_j^0 - x_j\|_{\Omega_j^{-1}}^2\right] \\ & + \frac{1}{2} \sum_i (q_i + 3) \log \left[1 + \frac{1}{q_i} \|y_i^0 - y_i\|_{\Phi_i^{-1}}^2\right] \end{aligned} \quad (4)$$

Table 1. Relative mean μ and standard deviation σ of MSE calculated over 1000 runs for L_2 -BA, L_2 -BA with the 2σ -edit rule (2σ -BA), and RST-BA, presented as: μ (σ). Error values for world points and camera XYZ parameters respectively are presented relative to the error incurred by L_2 -BA in the nominal case, shown in bold, i.e. where reprojection errors added were distributed as $N(0, 1)$.

| Noise Type | World Points | | | Camera XYZ | | |
|----------------------------|------------------|---------------|------------|------------------|---------------|------------|
| | L_2 -BA | 2σ -BA | RST-BA | L_2 -BA | 2σ -BA | RST-BA |
| $N(0, 1)$ | 1.0 (1.3) | 1.0 (1.2) | 1.0 (1.3) | 1.0 (0.9) | 0.8 (0.7) | 0.7 (1.4) |
| $.95N(0, 1) + .05N(0, 4)$ | 1.3 (1.6) | 1.2 (1.5) | 1.1 (1.4) | 6.3 (7.6) | 2.7 (4.1) | 3.5 (13.3) |
| $.9N(0, 1) + .1N(0, 4)$ | 1.5 (1.7) | 1.5 (1.9) | 1.4 (1.7) | 11.5 (12.5) | 5.6 (7.6) | 5.9 (18.1) |
| $.95N(0, 1) + .05N(0, 10)$ | 2.7 (3.4) | 1.8 (2.0) | 1.2 (1.4) | 69 (62) | 23 (27) | 7.3 (23) |
| $.9N(0, 1) + .1N(0, 10)$ | 3.6 (4.6) | 2.7 (3.0) | 1.4 (1.6) | 101 (76) | 49 (42) | 16.5 (34) |
| $.95N(0, 1) + .05N(0, 50)$ | 39 (45) | 21 (30) | 1.9 (1.7) | 580 (380) | 306 (242) | 12 (23) |
| $.9N(0, 1) + .1N(0, 50)$ | 60 (63) | 44 (47) | 2.5 (2.1) | 740 (510) | 470 (300) | 20 (36) |
| Student's t, df = 4 | 12.3 (13.5) | 12.2 (15.1) | 8.9 (10.2) | 240 (150) | 190 (130) | 38 (60) |

where s_{ij} , r_j , and q_i are known degrees of freedom parameters in model (3) associated to observations z_{ij} , prior camera parameters x_j^0 , and ground control points y_i^0 , respectively. The constants 2, 6 and 3 that appear in (4) are the dimensions of the pixel coordinates, camera poses, and world points, respectively.

Minimizing objective (4) provides maximum *a posteriori* (MAP) likelihood estimates for parameter vectors $\{x_j\}$ and $\{y_i\}$ in the Student's t model (3).

Now we describe an implicit trust region algorithm for minimizing (4). Given a sequence of column vectors $\{u_k\}$ and matrices $\{T_k\}$ we use the notation

$$\text{vec}(\{u_k\}) = \begin{bmatrix} u_1 \\ u_2 \\ \vdots \\ u_N \end{bmatrix}, \quad \text{diag}(\{T_k\}) = \begin{bmatrix} T_1 & 0 & \cdots & 0 \\ 0 & T_2 & & \vdots \\ \vdots & \ddots & \ddots & 0 \\ 0 & \cdots & 0 & T_N \end{bmatrix}$$

We define

$$c = \text{vec}(\{x_j\}, \{y_i\}).$$

We will now refer to objective (4) as $F(c)$. In order to minimize (4), we implement an iterative method of the form

$$\begin{aligned} \hat{c} &= c^k - (H^k)^{-1} \nabla F(c) \\ c^{k+1} &= \begin{cases} \hat{c} & \text{if } F(\hat{c}) < F(c^k) \\ c^k & \text{otherwise.} \end{cases} \end{aligned} \quad (5)$$

where k indexes the iterations, and H^k is a particular positive definite matrix described below, which one may think of as a Hessian approximation to $\nabla^2 F(c^k)$.

Let $J^k = [A^k \ B^k]$, where $A_{ij}^k = \partial_{x_j} h(x_j^k, y_i^k)$ and $B_{ij}^k = \partial_{y_i} h(x_j^k, y_i^k)$. Define weights

$$\begin{aligned} g_i^k &= \frac{q_i + 3}{q_i + \|y_i^0 - y_i^k\|_{\Phi_j^{-1}}} & \varrho_j^k &= \frac{r_j + 6}{r_j + \|x_j^0 - x_j^k\|_{\Omega_j^{-1}}} \\ \rho_{ij}^k &= \sqrt{\frac{s_{ij} + 2}{s_{ij} + \|\epsilon_{ij}^k\|_{\Sigma_{ij}^{-1}}}} \end{aligned} \quad (6)$$

Let $\tilde{A}_{ij}^k = \rho_{ij}^k A_{ij}^k$ and $\tilde{B}_{ij}^k = \varrho_j^k B_{ij}^k$. Let \tilde{A}^k and \tilde{B}^k be matrices with block components \tilde{A}_{ij}^k and \tilde{B}_{ij}^k , respectively, and define $\tilde{J}^k = [\tilde{A}^k \ \tilde{B}^k]$. Define

$$\begin{aligned} H^k &= (\tilde{J}^k)^T \Sigma^{-1} (\tilde{J}^k) + \text{diag}(\{\varrho_j^k \Omega_j\}) \\ &+ \text{diag}(\{g_i^k \Phi_i\}) + \lambda^k I \end{aligned} \quad (7)$$

where λ^k is a regularization parameter similar to the Levenberg-Marquardt method, and is updated according to the rule defined in Algorithm 3.16 of [18]. Specifically, λ increases quickly when the iteration (5) fails to improve the objective function (4), and otherwise is adjusted according to the rule

$$\lambda^{k+1} = \lambda^k \max\left(\frac{1}{3}, 1 - (2\phi^k - 1)^3\right) \quad (8)$$

where ϕ^k is the ratio of improvement predicted by the quadratic model with Hessian H^k to the actual improvement $F^k - F^{k+1}$.

From this presentation, it is clear that the RST-BA algorithm can be implemented by a simple reweighting of the data structures already present in L_2 -BA, and so RST-BA takes about the same time per iteration as L_2 -BA. The algorithm terminates when all the components of ∇F are below 10^{-6} . In practice, a hard iteration limit is set, since the problems are large and it is rarely necessary to solve them exactly. We followed this approach in testing and simulation.

5. Numerical Simulations

The RST-BA code used for the simulated and real tests is currently implemented as part of Nasa VisionWorkbench [10]. Since our target application is the reconstruction of the lunar surface from Apollo orbital imager data, our synthetic data was modeled in a similar context. Camera positions were generated in a sequence incremented along

the camera x -axis, with the z -axis of the camera coordinate system defined to point toward the lunar surface. The x -increment was calculated to yield the desired overlap between camera fields of view, to guarantee that each point on the surface was seen by at least two cameras. Given specifications for the camera elevation and location, a synthetic surface region was calculated, bounded by the camera field of view in the y -direction, the combined fields of view of the second through the penultimate cameras in the x -direction, and an estimate of minimum and maximum lunar surface height in the z -direction. 3-dimensional world points were then randomly generated within the volume bounded by this surface. Finally, each generated 3-dimensional point was projected into the image plane of each camera in which it was visible, giving a set of image coordinates for each point and camera pair.

After generation of the synthetic 3D world points, we added several kinds of noise to the ‘‘observations’’ made in the simulated system. In the lunar surface reconstruction context, observations include the image coordinates of each visible point, and extrinsic camera parameters that are known up with some precision from the Apollo mission telemetry. Our data generator perturbs image coordinates, camera positions, and camera pose according to nominal Gaussian distributions with specified variance in order to simulate measurement noise and camera uncertainty. To test the robustness of our algorithms against mistakes in the data, we also introduced outliers in the simulated errors according to error schemes we describe below.

1. Nominal conditions: The reprojection errors were generated using the normal distribution $\epsilon_{ij} \sim \mathbf{N}(0, 1)$.
2. Contaminated normal: The reprojection errors were generated using a mixture of two normals, i.e.,

$$\epsilon_{ij} \sim (1 - p)\mathbf{N}(0, 0.25) + p\mathbf{N}(0, \phi)$$

for values of $p \in \{0.05, 0.1\}$ and values of $\phi \in \{4, 10, 50\}$.

3. Student’s t -distribution: The reprojection errors were generated using Student’s t -distribution with $df = 4$.

For each run of each experiment, we ran the L_2 -BA algorithm as the baseline, along with L_2 -BA combined with a 2σ -edit rule (removing ‘outliers’ that were two standards of deviation away from the mean and refitting), and the RST-BA algorithm. All degrees of freedom parameters for RST-BA were set at 4 for all of the experiments.

The results for our simulated fitting are presented in Table 1. Each experiment was performed 1000 times, and we provide the relative median Mean Squared Error (MSE) value and standard deviation for the difference between ‘ground truth’ and the final estimates of the algorithms,

for the 3D world points data and for the camera location (x, y, z) data. We left the camera pose parameters fixed at their true values during the experiment, by placing a very strong prior on them. The relative MSE for the world points is defined by

$$\left(\frac{1}{N} \sum_{k=1}^N \|X_k - \hat{X}_k\|_2^2 \right) / (\mathbf{MSE}_0) \quad (9)$$

where N is the total number of 3D world points, X_k is the k -th ‘true’ world point, \hat{X}_k is the estimate, and \mathbf{MSE}_0 is the MSE of the baseline BA method in nominal conditions. The relative MSE measure for camera coordinates is similarly defined.

The L_2 -BA method with the 2σ -edit rule works as well or better than L_2 -BA alone. When the variance of the outliers is very large, the 2σ -edit rule cuts the relative error nearly in half, for both world points and camera parameters. The RST-BA algorithm works about as well as the 2σ -edit rule for cases with small outliers, but as the variance of the outliers grows, RST-BA cuts the relative error by a factor of 30 – an order of magnitude improvement over the 2σ -edit rule. When the errors are actually generated from the Student’s t -distribution, RST-BA cuts the camera error by a factor of 6 relative to the standard, and achieves a small improvement for the world points.

6. Bundle Adjustment in Orbital Imagery

To check the performance of the RST-BA algorithm on real data, we used imagery captured by the Apollo Metric Camera (AMC) on board the NASA Apollo 15 orbiter. The AMC is a frame camera with a 74 degree field of view that captured snapshots of the Moon’s surface at regular intervals. This resulted in overlap between images of 80%. The Apollo-era satellite tracking network was highly inaccurate by today’s standards, with errors estimated to be 2.04-km for satellite station positions and 0.002 degrees for pose estimates. This creates a need for refinement via bundle adjustment in order to create consistent 3D models between stereo pairs (see Figure 2). The specific frames processed were AS15-M-1089 through AS15-M-1159, which were part of Apollo 15’s 33rd orbital revolution[14].

In order to test the effectiveness of L_2 -BA against RST-BA, two datasets of image measurements were created:

1. *Processed Apollo tie-point data* was created with extensive processing and cleaning. First, tie points were automatically detected with the SURF [2] algorithm. Then outliers were removed using the RANSAC algorithm [5]. Finally the tie points were thinned down to 500 matches between pairs by removing the weakest matches while ensuring that the tie points remained evenly distributed across each image.

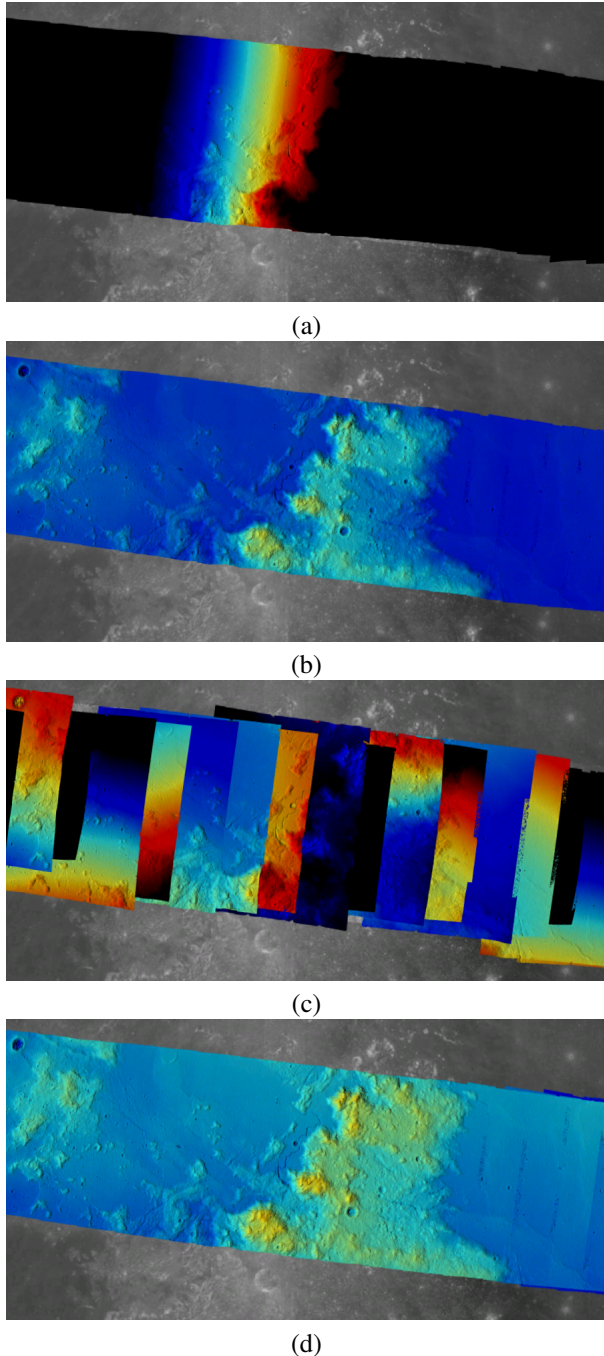


Figure 2. Surface reconstruction from Orbit 33 images. From top to bottom: (a) L_2 -BA, processed data set; (b) RST-BA, processed data set; (c) L_2 -BA, unprocessed data set; (d) RST-BA, unprocessed data set. Red indicates high elevation, blue indicates low elevation. Black indicates elevations out of the range of the color map. Ground control points were not used in these experiments.

2. *Unprocessed Apollo tie-point data* was created using the Interest Point detection algorithm based on SIFT [17]. No outlier rejection was done in this case, yield-

ing a data set with up to 50% outliers.

L_2 -BA and RST-BA were tested with both processed and unprocessed data sets. Results of these tests are shown in Table 2. Here, triangulation error is a measure of the average distance between the closest point of intersection of two forward projected rays for a set of tie-points. A decrease in triangulation error indicates a substantial improvement in the self-consistency of the DEMs in the data set.

After bundle adjustment was complete, we processed the imagery using stereo reconstruction tools [24] to produce dense topography of the lunar surface. This 3D reconstruction used the improved camera extrinsic parameters from bundle adjustment to produce a more consistent, seamless mosaic of 3D topographic models. Figure 2 shows these results with various bundle adjustment tests. Topography is represented by a color-map with red indicating high elevation and blue low elevation.

The original (unadjusted) camera parameters show clear discontinuities between adjacent models that are due to the uncertainties in the original Apollo tracking data. While *Processed* data yields reasonable results when ground control points are used, we did not use these points to emphasize that RST-BA can be used in their absence while L_2 -BA cannot. Without ground control points, L_2 -BA found a ‘kink’ in the DEM, which is responsible for the black sections visible in Figure 2 while RST-BA was able to reconstruct the DEM.

The results from the *unprocessed* data set, which contained nearly 50% outliers, show a stark difference between the two approaches. The L_2 -BA algorithm failed to create any improvement. Instead, the outliers caused severe and unpredictable distortion of the camera parameters. The RST-BA algorithm, on the other hand, was nearly unaffected, and produced results remarkably similar to those produced from the *processed* data set. Table 2 shows that median triangulation error were only slightly higher for the *unprocessed* data than they were for the *processed* data. This data suggests that RST-BA is significantly more robust to outliers than the standard bundle adjustment technique.

7. Conclusion

We have proposed RST-BA, a robust bundle adjustment algorithm, based on the Student’s t distribution, for performing bundle adjustment in the presence of outliers in tie-point matching. RST-BA preserves the sparse structure, and hence the speed, of L_2 -BA, and can be implemented by simple modifications to the L_2 -BA algorithm. Our test results on both synthetic and real data show that when the data have been preprocessed to remove outliers in the tie-point matches, RST-BA outperforms L_2 -BA by a small margin, and on unprocessed data with numerous outliers, RST-BA outperforms L_2 -BA by a significant margin. RST-BA

demonstrates significant advantages in both speed and accuracy of results over both L_2 -BA and L_2 -BA with a 2σ -edit rule, and can be used to reconstruct DEMs without data preprocessing and without ground control points. In future work, we will perform an extended comparison of RST-BA with “robust” methods such as Cauchy re-weighting in addition to the 2σ -edit rule. We will also work on the problem of estimating the degrees of freedom parameters, which are currently assumed to be known by the RST-BA algorithm.

8. Acknowledgements

We would like to thank our colleagues at the Arizona State University for supplying high resolution scans of the Apollo Metric Camera images. This work was funded by the NASA Lunar Advanced Science and Exploration Research (LASER) program grant #07-LASER07-0148, NASA Advanced Information Systems Research (AISR) program grant #06-AISRP06-0142, and by the NASA ESMD Lunar Mapping and Modeling Program (LMMP). We would also like to thank James Burke and Bradley Bell at the University of Washington for guidance in developing the optimization algorithm.

References

- [1] A. Aravkin. *Robust Methods with Applications to Kalman Smoothing and Bundle Adjustment*. PhD thesis, University of Washington, Seattle, WA, June 2010. [3](#)
- [2] H. Bay, A. Ess, T. Tuyetelaars, and L. Vangool. Speeded-up robust features (surf). *Computer Vision and Image Understanding*, 110(3):346, 2008. [5](#)
- [3] S. S. Brandt and U. Ziese. Robust alignment of transmission electron microscope tilt series. *Pattern Recognition, International Conference on*, 4:683–686, 2006. [2](#)
- [4] A. Cumani and A. Guiducci. Visual odometry for robust rover navigation by binocular stereo. In *Proc. WSEAS IC-SSIP*, 2006. [2](#)
- [5] M. A. Fischler and R. C. Bolles. Random sample consensus: a paradigm for model fitting with applications to image analysis and automated cartography. *Communications of the ACM*, 24(6):381, 1981. [5](#)
- [6] Fletcher. *Practical Methods of Optimization*. John Wiley and Sons, second edition, 1987. [3](#)
- [7] P. Fua. Regularized bundle-adjustment to model heads from image sequences without calibration data. *Int. J. Comput. Vision*, 38(2):153–171, 2000. [2](#)
- [8] P. Fua, R. Plaenkers, and D. Thalmann. From synthesis to analysis: Fitting human animation models to image data. *Computer Graphics International Conference*, 0:4, 1999. [2](#)
- [9] N. Fukaya, T. Anai, H. Sato, N. Kochi, M. Yamada, and H. Otani. Application of robust regression for exterior orientation of video images. In *ISPRS08*, 2008. [2](#)
- [10] M. Hancher, M. Broxton, T. Fong, and Contributors. [NASA VisionWorkbench](https://github.com/visionworkbench/visionworkbench). <https://github.com/visionworkbench/visionworkbench>. [4](#)
- [11] R. I. Hartley and A. Zisserman. *Multiple View Geometry in Computer Vision*. Cambridge University Press, ISBN: 0521540518, second edition, 2004. [2](#), [3](#)
- [12] R. I. Hartley and A. Zisserman. *Multiple View Geometry in Computer Vision*. Cambridge University Press, ISBN: 0521540518, second edition, 2004. [2](#)
- [13] Q. Ke and T. Kanade. Quasiconvex optimization for robust geometric reconstruction. In *IEEE International Conference on Computer Vision (ICCV 2005)*, volume 2, pages 986–993, October 2005. [2](#)
- [14] S. Lawrence, M. Robinson, M. Broxton, J. Stopar, W. Close, J. Grunsfeld, R. Ingram, L. Jefferson, S. Locke, R. Mitchell, T. Scarsella, M. White, M. Hager, T. Watters, E. Bowman-Cisneros, J. Danton, and J. Garvin. The apollo digital image archive: New research and data products. In *Proceedings of the NLSI Lunar Science Conference*, page 2066, 2008. [5](#)
- [15] T. Lee. Robust 3d street-view reconstruction using sky motion estimation. In *Proceedings of the IEEE International Workshop on 3-D Digital Imaging and Modeling (3DIM2009) in conjunction with ICCV*, October 2009. [2](#)
- [16] M. Lourakis and A. Argyros. Sba: A software package for sparse bundle adjustment. *ACM Transactions on Mathematical Software*, 36(1):30, 2009. [2](#), [3](#)
- [17] D. G. Lowe. Distinctive image features from scale-invariant keypoints. *International Journal of Computer Vision*, 60(2):91, 2004. [6](#)
- [18] K. Madsen, H. Nielsen, and O. Tingleff. *Methods for Non-Linear Least Squares Problems*. Technical University of Denmark. Springer, 2nd edition, 2004. [2](#), [3](#), [4](#)
- [19] R. A. Maronna, D. Martin, and Yohai. *Robust Statistics*. Wiley Series in Probability and Statistics. John Wiley and Sons, 2006. [2](#), [3](#)
- [20] H. Mayer. Robust least-squares adjustment-based orientation and auto-calibration of wide-baseline image sequences. In O. Hellwich, I. Niini, C. Ressler, V. Rodehorst, D. Scharstein, and P. Sturm, editors, *Towards Benchmarking Automated Calibration, Orientation and Surface Reconstruction from Images*, Beijing, China, 2005. ICCV 2005. [2](#)
- [21] H. Mayer. 3d reconstruction and visualization of urban scenes from uncalibrated wide-baseline image sequences (mayer) 2006. In *IAPRS Volume XXXVI, Part 5*, Dresden, 2006. [2](#)
- [22] H. Mayer, M. Mosch, and J. Peipe. Comparison of photogrammetric and computer vision techniques - 3d reconstruction and visualization of wartburg castle. In *CIPA 2003 19th International Symposium*, pages 103–108, Antalya, 2003. [2](#)
- [23] E. Mouragnon, M. Lhuillier, M. Dhome, F. Dekeyser, and P. Sayd. Generic and real-time structure from motion using local bundle adjustment. *Image and Vision Computing*, 27(8):1178–1193, 2009. [2](#)
- [24] A. Nefian, K. Husmann, M. Broxton, V. To, M. Lundy, and M. Hancher. A bayesian formulation of sub-pixel refinement in stereo orbital imagery. In *Int’l Conf on Image Processing*, 2009. [6](#)
- [25] J. Nocedal and S. J. Wright. *Numerical Optimization*. Springer Series in Operations Research. Springer, 1999. [3](#)

| Dataset | Algorithm | Start Triangulation Error | | | End Triangulation Error | | |
|-------------|-----------|---------------------------|--------|--------|-------------------------|---------------|--------|
| | | Min | Median | Max | Min | Median | Max |
| Processed | L_2 -BA | 0.0616 | 714.18 | 134234 | 0.0008 | 36.309 | 178636 |
| | RST-BA | 0.0616 | 714.18 | 134234 | 0.0002 | 14.329 | 132966 |
| Unprocessed | L_2 -BA | 0 | 729.87 | 239452 | 0 | 4409.9 | 242179 |
| | RST-BA | 0 | 729.87 | 239452 | 0 | 14.404 | 240647 |

Table 2. Triangulation errors for the Apollo DEM reconstruction, using *processed* and *unprocessed* Apollo tie-point data. RST-BA performs much better than L_2 -BA for *unprocessed* data, and better than L_2 -BA for *processed* data.

- [26] G. Seber and C. Wild. *Nonlinear Regression*. John Wiley and Sons, 1988. [3](#)
- [27] N. Sünderhauf, K. Konolige, S. Lacroix, and P. Protzel. Visual odometry using sparse bundle adjustment on an autonomous outdoor vehicle. In P. Levi, M. Schanz, R. Lafrenz, and V. Avrutin, editors, *AMS, Informatik Aktuell*, pages 157–163. Springer, 2005. [2](#)
- [28] B. Triggs, P. F. McLauchlan, R. I. Hartley, and A. W. Fitzgibbon. Bundle adjustment - a modern synthesis. In *ICCV '99: Proceedings of the International Workshop on Vision Algorithms*, pages 298–372, London, UK, 2000. Springer-Verlag. [1](#), [2](#)
- [29] J. Zhang, M. Boutin, and D. G. Aliaga. Robust bundle adjustment for structure from motion. In *Image Processing, 2006 IEEE International Conference on*, pages 2185–2188, Oct. 2006. [2](#)